Core-SOL Modelling of Neon Seeded JET Discharges with the ITER-like Wall*

G. Telesca[1][**], **I. Ivanova-Stanik**[2], **R. Zagórski**[2], **S. Brezinsek**[3], **A. Czarnecka**[2], **P. Drewelow**[4], **C. Giroud**[5], **A. Huber**[3], **S. Wiesen**[3], and **JET EFDA contributors**[***]

 EUROfusion Consortium, JET, Culham Science Centre, Abingdon, OX14 3DB, UK

[1] Department of Applied Physics, Ghent University, B-9000 Gent, Belgium
[2] Institute of Plasma Physics and Laser Microfusion, Warsaw, Poland
[3] Forschungszentrum Jülich GmbH, Institut für Klima-und Energieforschung-Plasmaphysik- 52425, Jülich, Germany
[4] Max-Planck-Institut für Plasmaphysik, D-17491 Greifswald, Germany
[5] CCFE Culham, Abingdon, Oxon. OX14 3DB, UK

Five ELMy H-mode Ne seeded JET pulses have been simulated with the self-consistent core-SOL model COREDIV. In this five pulse series only the Ne seeding rate was changed shot by shot, allowing a thorough study of the effect of Ne seeding on the total radiated power and of its distribution between core and SOL to be made. The increase in the simulations of the Ne seeding rate level above that achieved in experiments shows saturation of the total radiated power at a relatively low radiated-heating power ratio ($f_{rad} = 0.60$) and a further increase of the ratio of SOL to core radiation, in agreement with the reduction of W release at high Ne seeding level. In spite of the uncertainties caused by the simplified SOL model of COREDIV (neutral model, absence of ELMs and slab model for the SOL), the increase of the perpendicular transport in the SOL with increasing Ne seeding rate, which allows to reproduce numerically the experimental distribution core-SOL of the radiated power, appears to be of general applicability.

1 Introduction

For a full metallic device like JET with the ITER-Like-Wall (W divertor, Be wall) impurity seeding is an essential technique to reduce the power load to the targets, via enhanced edge radiation. Indeed, the naturally occurring radiation losses are low ($\sim$ 25-30% of the heating power), as compared to those with carbon target ($\sim$ 50%). Among quite a number of experiments recently carried out at JET to implement impurity seeding scenarios (with N, Ne and Ar), a series of five H-mode ELMy pulses has been selected for a thorough study of transport and radiation features of neon seeded discharges. In fact, differently from other experiments, in this five pulse series the basic plasma parameters (density and heating power) have been kept nearly constant [1], except for the neon seeding rate. This may allow understanding the global effect of neon seeding with increasing radiation level.

The experiments were performed in the ITER-relevant high-triangularity, vertical-target configuration, at $I_p = 2.5$ MA and $B_t = 2.7$ T. The D puffing rate was maintained constant at 4.1×10^{22} e/s (leading to avolume average density, $\langle n_e \rangle$, in the range 8 - 8.7 $\times 10^{19}$ m^{-3}) and the auxiliary heating power was about 18 MW NBI + 4-5 MW ICRF heating. The neon seeding rate was increased pulse by pulse resulting in the increase of the total radiated power (P_{rad}^{TOT}) in the range 9.5 to 13 MW. It was observed that this leads also to the increase, pulse by pulse, of the ratio between the radiated power in the divertor (P_{rad}^{DIV}) to (P_{rad}^{TOT}). (Please, note that, from bolometric signals, the core radiation is predominantly emitted at the edge of the confined plasma). Numerical

---

simulation of these five discharges has been made also in view of extrapolating a scaling for neon seeding, based on experimental JET data.

2   The COREDIV code

For the simulations we have used COREDIV code [2], which self-consistently couples the plasma core with the plasma edge and the main plasma with impurities. In particular, the code has proved its capability of reproducing the main features of the core as well as of the SOL JET discharges both with carbon and with the ILW [3]. Although the simulations refer to the inter-ELM phase of the discharges, since production as well as flushing out of W due to ELMs is not accounted for in the present model, the numerical results might be compared with experimental data averaged over several ELM periods. In fact, an "ad hoc" increase in COREDIV of the W yield by a factor of 1.4 is seen to be sufficient to lead to a good match between calculated and time-averaged W fluxes [4].

In the core, given as code input the volume average electron density $\langle n_e \rangle$, the 1D radial transport equations for bulk ions, for each ionization state of impurity ions and for the electron and ion temperature are solved. The electron ion energy fluxes are defined by the local transport model proposed in ref. [5] which reproduces a prescribed energy confinement law. In particular, the anomalous heat conductivity is given by the expression $\chi_{e,i} = C_{e,i} \left(a^2/\tau_E \right) \times F(r)$ where r is the radial coordinate, a is the plasma radius, τ_E is the energy confinement time defined by the ELMy H-mode scaling law and the coefficient ($C_e = C_i$) is adjusted to have agreement between calculated and experimental confinement times. The parabolic-like profile function $F(r)$, which may be slightly change from run to run in order to match with the actual profiles of the experimental pulse to be modelled, can be modified at the plasma edge to provide for a transport barrier of chosen level. The main plasma ion density is given by the solution of the radial diffusion equation with diffusion coefficients $D_i = D_e = 0.2 \, \chi_e$, as in ref. [5]. Note, however, that the solution of the diffusion equation is largely independent of the exact value of D_e/χ_e. Indeed, a change in D_e/χ_e causes a consistent change in the source term, since the average electron density is a COREDIV input. For the auxiliary heating, parabolic-like deposition profile is assumed $P_{aux}(r) = P_0 \left(1 - r^2/a^2 \right)^y$ where y is in the range 1.5-3, depending on the quality of the auxiliary heating, NBI or/and ICRF.

In consideration of the significant fraction of ICRF heating used and of the absence of any tendency to impurity accumulation in the presently examined pulses, the numerical radial impurity transport is described by anomalous diffusion only, without pinch.

In the SOL we use the 2D boundary layer code EPIT, which is primarily based on Braginskii-like equations for the background plasma and on rate equations for each ionization state of each impurity species [6]. An analytical description of the neutrals is used, based on a simple diffusive model. COREDIV takes into account the plasma (D, Be and seeded impurities) recycling in the divertor as well as the sputtering processes at the target plates including deuterium sputtering, self-sputtering and sputtering due to seeded impurities. (For deuterium and neon sputtering and tungsten self-sputtering the yields given in refs. [7, 8] are used). The recycling coefficient is an external parameter which in COREDIV depends on the level of the electron density at the separatrix, n_{e_sep}, given as an input and increases with increasing n_{e_sep}.

A simple slab geometry (poloidal and radial directions) with classical parallel transport and anomalous radial transport ($D_{SOL} = \chi_i = 0.5 \, \chi_e$, where χ_e ranges typically 0.5-1 m²/s), is used and the impurity fluxes and radiation losses by impurity ions are calculated fully self-consistently. Although the values of the transport coefficients in the SOL are generally comparable to those at the separatrix, in the present simulations the value of D_{SOL} is set arbitrarily (in the range 0.2-0.4 m²/s) in order to match with the core-SOL distribution of the radiated power, depending on the different levels of Ne seeding rate (see next section). All the equations are solved only from the midplane to the divertor plate, assuming inner-outer symmetry of the problem. This implies that the experimental in - out asymmetries, observed especially at high density-high radiation level, are not reproduced in COREDIV results. However, for all the different situations examined so far (with carbon plates and with the ILW, and with different seeding levels) the COREDIV numerical reconstructed total radiation in the SOL matches well with the total experimentally measured SOL radiation, indicating that for JET conditions the edge-core COREDIV modelling can describe the global trend of this important quantity.

3   Experimental data and simulations

Figure1 shows the tomographic reconstruction from bolometric data for one of the pulses considered. It is apparent that a clear limit between the radiation emitted in the core and that in the SOL is difficult to define within the uncertainties in space and absolute numbers of the measurement (order of 20%), especially in the vicinity of the x-point. Therefore, we have followed a procedure, used at JET [9], by which all the power radiated below $Z = -1$ m is considered as divertor radiation. Since neon radiates partly in the SOL and partly at the very edge of the plasma core around the X-point [10], this assumption turns out to include the total radiation emitted by Ne in what we call "experimental divertor radiation". Being the core module of COREDIV one-dimensional (see above), the simulated Ne radiation inside the separatrix is poloidally uniformly distributed and it is located, as in the experiment, at the very edge of the core (see Fig. 2). To compare consistently simulations with measurements we have therefore added the COREDIV neon radiation emitted at the very edge of the core to the COREDIV SOL radiation, resulting in the "simulated divertor radiation".
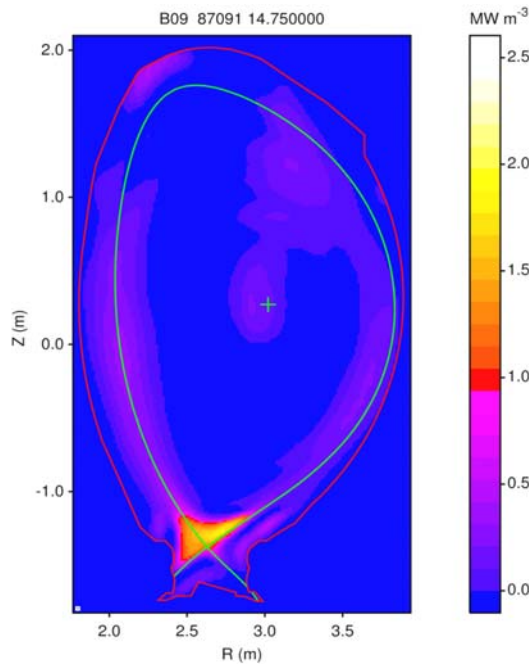

Fig. 1 Bolometric tomographic reconstruction of the radiated power for JPN 87091, $t = 14.75$ s.
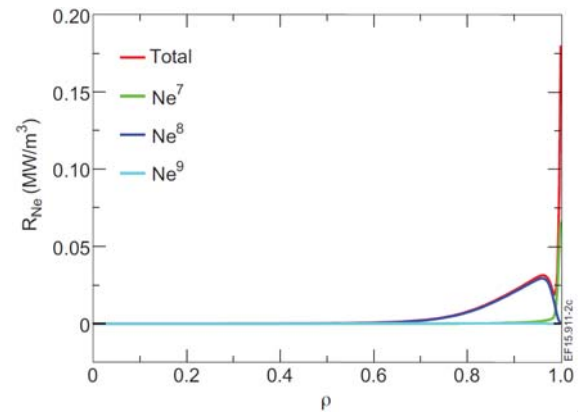
Fig. 2 COREDIV reconstruction of the radiated power by Ne in the plasma core for JPN 87091.

    Each of the 5 pulses considered has been simulated with acceptable accuracy (see, for example the comparison experiment-simulation for the core temperature and density profiles of one of them, Fig. 3), but since the 5 pulses are similar but not identical in electron density and auxiliary power, P_{aux}, the input density $\langle n_e \rangle$ as well as the input P_{aux} level had to be slightly adjusted for each pulse. However, it turned out to be impossible to reproduce numerically the experimental P_{rad}^{TOT} and its distribution between core and SOL for the 5 pulses by changing only Γ_{Ne}, together with the little changes in $\langle n_e \rangle$ and P_{aux} above mentioned. One solution was found by increasing the COREDIV input perpendicular anomalous diffusivity coefficient in the SOL, D_{SOL}, from 0.22 to 0.34 m²/s with increasing the experimental Γ_{Ne} from 0.1 to 1.06×10^{22} el/s. Note that Γ_{Ne} which is given as COREDIV input and which numerically reproduces the experimental P_{rad}^{TOT} and P_{rad}^{DIV} values is about a factor of 8 lower than that in the experiment. This is due to two reasons : i) in contrast with the experiment, in COREDIV all the neon atoms injected enter the plasma and ii) Ne recycling coefficient in COREDIV is set $R = 0.925$, which might be significantly higher that the effective experimental one considering also the action of the out-puffing gas valve. In the following, we will refer to the COREDIV Ne fluxes.

    With increasing the Ne seeding rate, P_{rad}^{TOT} increases, from 9.5 MW to 13 MW, as does the ratio $P_{rad}^{DIV}/P_{rad}^{TOT}$, from 0.23 to 0.36, both in experiments and in simulations, and the electron temperature at the outer target, T_{e_pl},

decreases from about 9 to 4-5 eV, in agreement with the simulations (see Fig. 4). Please, note the slight increase in the slope of the curve $P_{rad}^{DIV}/P_{rad}^{TOT}$ at about $\Gamma_{Ne} = 1 \times 10^{21}$ el/s due to a strong reduction of W sputtering at T_{e_pl} at about 5 eV. While from LP measurements the D fluxes to the plate decrease from 4.5 to 1.5×10^{23} 1/s with increasing Γ_{Ne}, in the simulations they increase from about 5 to 7×10^{23} 1/s. Although the reason for this disagreement is not fully clear yet, it may partly depend on the self-consistent model of core-SOL we have used in COREDIV. Indeed, during the D_{SOL} scan, the simulated particle fluxes core-SOL decrease (screening effect), resulting in the self-consistent increase of the simulated recycling fluxes Γ_D in order to maintain constant the density at the separatrix (given as code input and kept constant in these scans, $n_{e\_sep} = 0.45 \langle n_e \rangle$). In fact, some test runs have shown that the COREDIV simulated Γ_D decrease with increasing D_{SOL} if the input n_{e_sep} is reduced simultaneously. More in general, this disagreement shows that, due to the simplified neutral model, the determination of the ionization front in situations close to detachment is outside the limits of applicability of COREDIV.
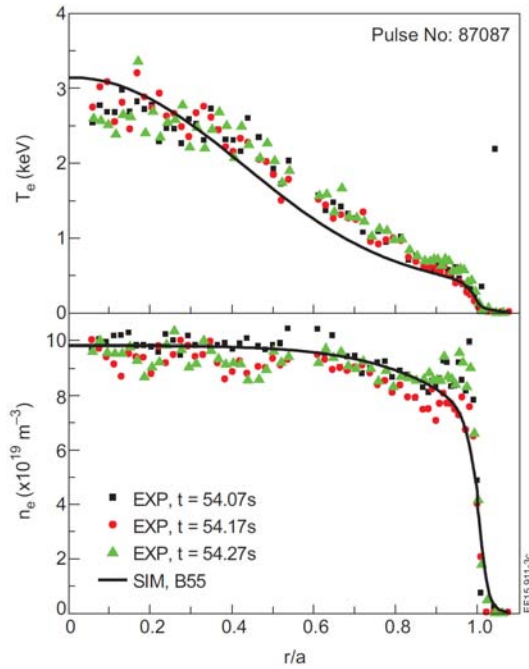

Fig. 3 Comparison of experimental (from HRTS, $t = 14.17$ s) and simulated temperature and density profiles for JPN 87087.

The numerical tungsten concentrations, c_W, first increase then decrease with increasing Γ_{Ne}, in qualitative agreement with spectroscopic VUV measurements (Fig. 5). This trend reflects the temperature dependence of the W sputtering yield by Ne, which vanishes for T_{e_pl} below 4-5 eV [8].

Since we are mostly interested in producing a scaling based on experiments, also to predict global trends, we have increased the COREDIV Ne seeding rate up to $\Gamma_{Ne} = 2 \times 10^{21}$ el/s and we have added the case for $\Gamma_{Ne} = 0$ for two slightly different densities ($\langle n_e \rangle = 8.7$ and 8.0×10^{19} m^{-3}), keeping $P_{aux} = 23$ MW. All the input parameters, but Γ_{Ne} and D_{SOL}, were maintained constant in these scans. On the basis of the numerical results shown in Figs. 4 and 5 the following considerations can be done.

The quick increase of P_{rad}^{TOT} and of c_W together with the drop of $P_{rad}^{DIV}/P_{rad}^{TOT}$ for Γ_{Ne} between 0 and 0.2×10^{21} el/s shows that the main effect of Ne seeding at high T_{e_pl} is tungsten release (and core radiation) with marginal effect on the radiated power in the SOL.

The computed very slow increase of P_{rad}^{TOT} with increasing Γ_{Ne} for $\Gamma_{Ne} > 1.5 \times 10^{21}$ 1/s, which tends to vanish for f_{rad} about 0.6 (see also Ref. [11]), occurs in the experimental pulses with ELM activity, as in those here considered. In the case of loss of ELMs, or strong reduction of their frequency, the experimental P_{rad}^{TOT} may keep increasing significantly, due to higher W dwell time [9]. Modelling of such pulses would require the neoclassical pinch term to be included in the COREDIV impurity transport model, see Sect. 2.

In parallel with the quick increase of P_{rad}^{TOT} with increasing Γ_{Ne} at low Γ_{Ne}, the power to the plate drops also quickly. In contrast, at high Γ_{Ne} the rate of change of P_{rad}^{TOT} with increasing Γ_{Ne} is marginal as is that of the power to the plate. Therefore, since with increasing Γ_{Ne} also Z_{eff} increases, see Fig. 5, a careful analysis

of advantages (reduction of P_{plate}) and disadvantages (increase in Z_{eff}) has to be done to establish the most appropriate neon seeding level in terms of the overall performances.

It is worth mentioning that impurity seeding experiments at JET have been carried out also with nitrogen and COREDIV modelling has been successfully performed, see for example refs. [3, 12]. Apart from the obvious difference in recycling behaviour, the basic trends of nitrogen seeding regarding radiation and contamination have been found to be rather similar to those of neon, both in experiments and in simulations, as expected, considering the little difference in the atomic number of N and Ne. While COREDIV is also capable to perform simulations with argon seeding, see for example ref. [13], the few and occasional JET experiments with Ar seeding performed so far do not allow yet a serious comparison JET experiments-COREDIV modelling to be done.
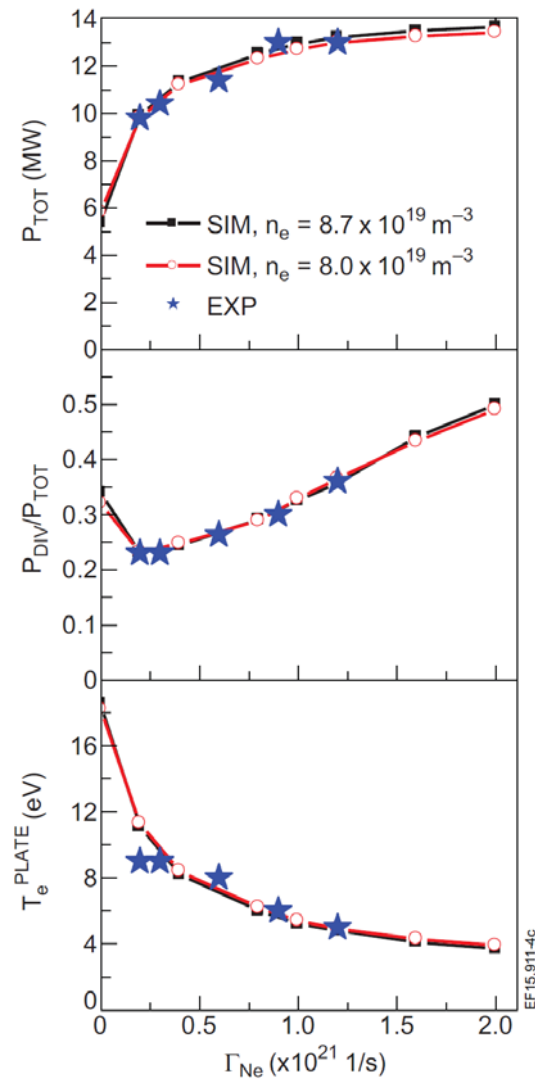

Fig. 4 Experimental and COREDIV simulated (from top to bottom) total radiated power, ratio of radiated power in the divertor and the total one, electron temperature at the target plate as a function of the COREDIV Ne seeding rate (please, see text).
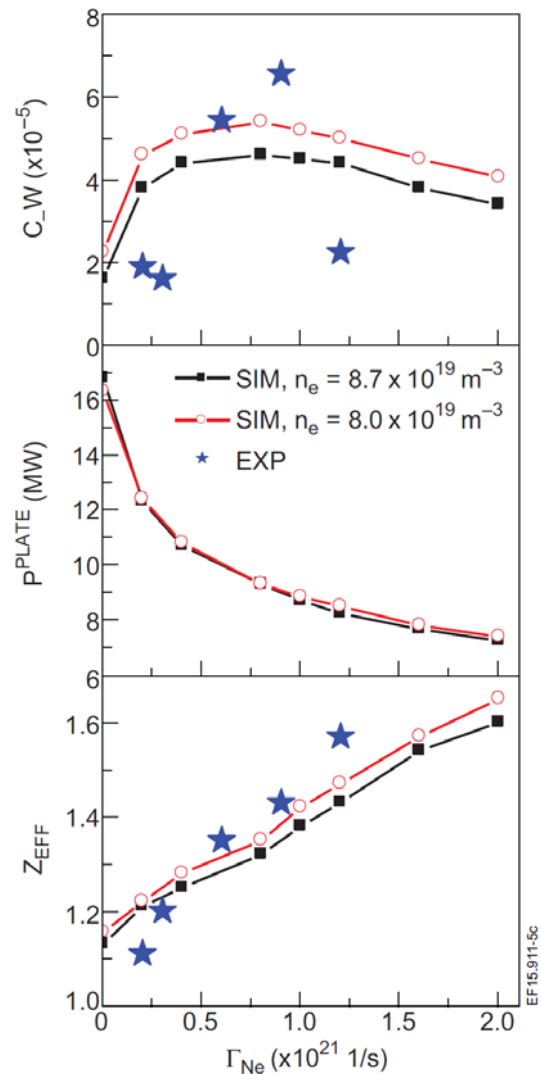
Fig. 5 Experimental and COREDIV simulated (from top to bottom) W concentration, power to the target plate and Z_{eff} as a function of the COREDIV Ne seeding rate (please, see text).

4 Summary

Within the uncertainties of the present simulations, caused mainly by the simplified neutral model and by the absence of ELM modelling, the main experimental trends of Ne seeded in JET with the ILW have been numerically reconstructed. Indeed, even though the actual dynamic of ELMs (W production, flushing out and transport) is bypassed by the assumptions of the steady-state W source and the W anomalous transport in the core, the simulated radiated power as well as the W concentration match well experimental data, showing the rollover in the W concentration with increasing Ne seeding level. To reproduce correctly the total radiated power and its distribution core-SOL for each examined pulse, the perpendicular particle transport coefficient in the SOL had to be increased with increasing the Ne seeding rate, this representing a significant new finding of the present study. Extension of the above procedure to Ne seeding rates higher than in experiment leads only to a marginal increase in the total radiated power, due to the reduced core radiation (reduced W production) compensated by the increase of radiation in the SOL at low target temperature and high particle transport. The positive effect of Ne seeding on the power to the plate, which decreases significantly, is partly balanced by the increase in Z_{eff}.

References

[1] C. Giroud et al, 25th IAEA Fusion Energy Conference, St.Petersburg, Russia, 2014, EX/P5-25.
[2] R. Zagorski et al., Contrib. Plasma Phys. **48**, 179 (2008).
[3] G. Telesca et al, J.Nucl. Mater. **463**, 577 (2015).
[4] G. Telesca et al, Contrib. Plasma Phys. **54**, 347 (2014).
[5] J. Mandrekas and W.M. Stacey, Nucl. Fusion. **35**, 843 (1995).
[6] S.I. Braginskii, Rev. Plasma Phys. **1**, 205 (1965).
[7] Y. Yamamura et al, Report of the IPP Nagoya, IPPJ-AM-26 (1083).
[8] C. Garcia-Rosales et al., J. Nucl. Mater. **218**, 8 (1994).
[9] A. Huber et al., 41st EPS Conference on Plasma Physics, P1.031 (2014).
[10] M. Wischmeier, 25th IAEA Conference, St. Petersburg, Russia, 2014, EX/7-2.
[11] R. Zagorski et al., J. Nucl. Mater. **463**, 649 (2015).
[12] G. Telesca et al., Plasma Phys. Control. Fusion **53**, 115002 (2011).
[13] I. Ivanova-Stanik and R. Zagorski, Nucl. Fusion **55**, 073034 (2015).